DOI: 10.1002/ejic.200700095

A Magnetostructural and Electrochemical Study of Cu^{II} and Fe^{III} Complexes Containing a Tetradentate Aminebis(phenolate) Ligand with a Pendent Tetrahydrofuran Group

Elham Safaei,[a] Thomas Weyhermüller,[a] Eberhard Bothe,[a] Karl Wieghardt,[a] and Phalguni Chaudhuri*[a]

Keywords: Iron / Copper / Aminebis(phenol) / Electrochemistry / Magnetism

Ligating properties of a tetradentate ligand 2-{bis[(3,5-di-*tert*-butyl-2-hydroxybenzyl)amino]methyl}tetrahydrofuran, H_2L, with [O,O,N,O]-donor atoms towards Cu^{II} and Fe^{III} are described. The ligand H_2L yields both mononuclear LFe^{III}(acac) (**1**) and dinuclear $[L_2Fe^{III}{}_2(\mu\text{-}OCH_3)\text{-}(\mu\text{-}OH)]$ (**2**), $[L_2Fe^{III}{}_2(\mu\text{-}C_2O_4)]$ (**3**) and $[L_2Cu^{II}{}_2]$ (**4**) complexes, which were characterized by various physical techniques, including X-ray diffraction, Mössbauer, electrochemical and magnetic susceptibility (2–290 K) measurements. That the electrochemical oxidations are ligand-centered, i.e. formation of phenoxyl radicals from the coordinated phenolates, have been shown by voltammetric methods. Complexes **2**–**4** display antiferromagnetic exchange coupling of the neighbouring metal centers. Comparison of the evaluated weak exchange coupling constants (J) with the literature values leads to the conclusion that the angle Cu–O–Cu′ is not the only determinant for the nature of the exchange coupling and the capability of the bridging ligands as mediators for spin coupling in case of Fe^{III} follows the order phenoxide ≈ methoxide > hydroxide.

Introduction

The amino acid tyrosine and its one-electron oxidized tyrosyl radical are quite common at the active centers of metalloenzymes involved in oxygen-dependent enzymatic radical catalysis.[1] Copper-containing galactose oxidase (GO), iron-containing ribonucleotide reductase (RR) are just two examples among others. This finding has elicited the interest of bioinorganic chemists in using phenol-containing ligands to mimic both structure and function of such metalloenzymes.[2] In this area, we have reported some bioinspired complexes as functional models of metalloenzymes[3] viz. galactose oxidase, catechol oxidase, and amine oxidases. These low-molecular weight complexes exhibit catalytic activity for aerial oxidation of organic substrates like alcohols, amines and catechols.

In continuation of our continuing interest in aminebis(phenol) ligands with O,N,O-donor atoms[4] and with the aim to scrutinize the effect of an additional pendent arm on the ligating property of the resulting tetradentate ligand towards transition metals, we argued for a weak-field donor pendent arm containing an ether group. An obvious choice is a tetrahydrofuran pendent arm. Thus the ligand H_2L was selected for the investigation.

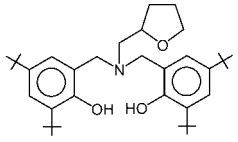

H_2L

Such aminebis(phenol) ligands with different pendent arms, such as amines with tetrahydrofuran, have already been used in the field of phosphorus chemistry[5] and for catalytic olefin polymerization involving group IV metal complexes.[6] Scheme 1 shows the complexes prepared with the ligand H_2L together with the labels. We report herein the synthesis, the structural, spectroscopic and magnetic properties of complexes $[LFe^{III}(acac)]$ (**1**), $[L_2Fe^{III}{}_2(\mu\text{-}OCH_3)(\mu\text{-}OH)]$ (**2**), and $[L_2Fe^{III}{}_2(\mu\text{-}C_2O_4)]$ (**3**). The dinuclear Cu^{II} complex $[L_2Cu^{II}{}_2]$ (**4**) will also be described.

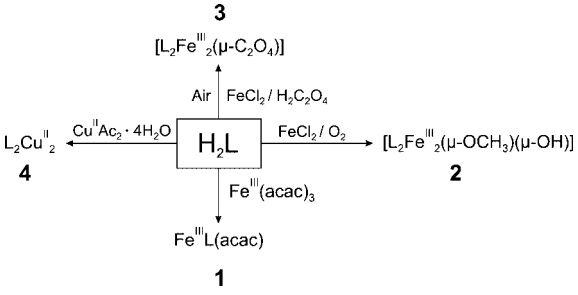

Scheme 1.

[a] Max-Planck-Institute for Bioinorganic Chemistry
Stiftstraße 34–36, 45470 Mülheim an der Ruhr, Germany
E-mail: Chaudh@mpi-muelheim.mpg.de

Results and Discussion

The ligand 2-{bis[(3,5-di-*tert*-butyl-2-hydroxybenzyl)-amino]methyl}tetrahydrofuran, H_2L, was prepared according to a procedure reported in the literature.[6b] The purity of the ligand was checked by liquid chromatography to be 98.7%. The IR, ^1H NMR and MS data are in agreement with the literature data (see Experimental Section), no further discussion is necessary here. To gain insight into the metrical parameters of the ligand, we have determined the structure of the ligand by X-ray diffractometry. Figure 1 displays the structure of the ligand H_2L in the solid state. The X-ray analysis of single crystals of H_2L, performed at 100 K, reveals moderate hydrogen bonding between the phenolic hydroxy group O(15) and the ether group O(1) of the tetrahydrofuran ring, whereas the second phenolic group O(23) and the amine nitrogen N(7) are hydrogen-bonded [O(15)···O(1) 2.786 Å and O(23)···N(7) 2.731 Å]. The bond lengths and angles for the ligand, listed in Table 1, seem reasonable and do not warrant any special discussion.

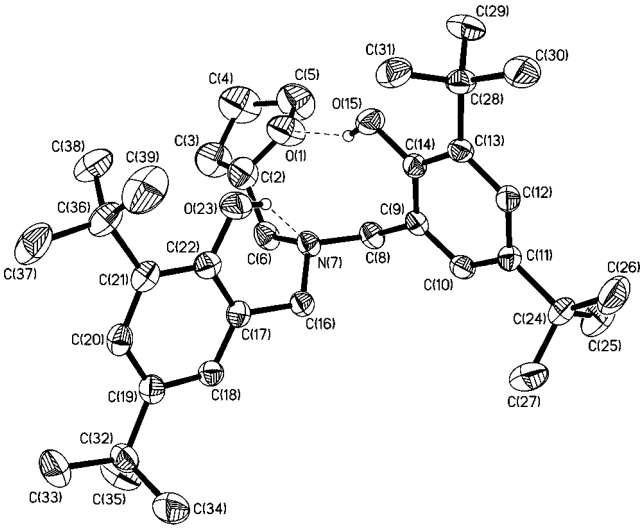

Figure 1. ORTEP representation for the amine bis (phenolato) THF ligand(L) (thermal ellipsoid probability 40%).

Methanolic solutions of H_2L were treated with metal salts, Et_3N and an additional ligand in some cases in suitable ratio and the solutions were heated at reflux to yield the complexes **1**–**4** in good yields. EI mass spectrometry was helpful in detecting the mononuclear nature for **1** and the dinuclear nature for **2**–**4**. The molecular ion peaks at *m*/*z* 690 (47.7%) for **1**, at *m*/*z* 1198 (11%) for **4** and *m*/*z* 1270 (47%) for **3** were observed. The signal at *m*/*z* 1198 (intensity about 12%) for **2** supports the dinuclear nature of **2**.

The ν(OH) stretch for the pure ligand, strong and sharp at 3372 cm^{-1}, vanishes after complex formation and is replaced by a very broad signal indicating the coordination of the phenol group to the metal. For **1** the most relevant features occur at 1598 and 1519 cm^{-1} corresponding to the ν(C=O) of the coligand acetylacetonate (acac). A new peak at 1067 cm^{-1} observed for **2** is ascribed to the ν(OCH_3) group of the bridging methoxide ligand. Complex **3** exhibits strong to moderate vibrations at 1655 cm^{-1} ($\nu_{as}OCO$), 1400 cm^{-1} (ν_sOCO) and 837 cm^{-1} ($\nu_\delta OCO$) as has been observed earlier for similar oxalate-bridged complexes.[7] Selected IR data for complexes **1**–**4** are given in the Experimental Section.

Table 1. Selected bond lengths [Å] and angles [°] for the ligand H_2L.

O(1)–C(2)	1.377(4)
O(1)–C(5)	1.458(5)
N(7)–C(6)	1.480(4)
N(7)–C(16)	1.473(2)
N(7)–C(8)	1.480(2)
O(23)–C(22)	1.366(2)
O(15)–C(14)	1.373(2)
C(14)–C(13)	1.403(3)
C(13)–C(12)	1.398(3)
C(12)–C(11)	1.397(3)
C(11)–C(10)	1.382(3)
C(10)–C(9)	1.383(3)
C(9)–C(14)	1.399(3)
C(22)–C(21)	1.406(3)
C(21)–C(20)	1.385(3)
C(20)–C(19)	1.391(3)
C(19-C(18)	1.394(3)
C(18)–C(17)	1.385(3)
C(17)–C(22)	1.402(3)
C82)–O(1)–C(5)	110.2(3)
C(16)–N(7)–C(6)	114.1(2)
C(16)–N(7)–C(8)	109.8(2)
C(8)–N(7)–C(6)	111.9(6)
O(23)–C(22)–C(17)	119.9(2)
O(23)–C(22)–C(21)	119.7(2)
O815)–C(14)–C(13)	118.2(2)
O(15)–C(14)–C(9)	121.0(2)

X-ray Diffraction Studies of 1, 2, 3 and 4

Single crystals of deep red [LFe(acac)]·$C_2H_5OC_2H_5$ (**1**) were obtained from an ethereal solution by slow evaporation. As no substantial differences in bond lengths and angles are found for the two crystallographically non-equivalent molecules, only one ORTEP diagram for the structure of compound **1** is displayed in Figure 2. Selected bond lengths and angles are summarized in Table 2. The overall geometry around the iron ion Fe(1) is best described as a distorted octahedron with two *cis* positioned oxygens O(41) and O(45) of the acetylacetonato coligand acac, whereas the doubly deprotonated tripodal ligand $[O\cap N(O)\cap O]^{2-}$ occupies the remaining four coordination sites. All the phenyl rings attached to the phenolate oxygen atoms are found to be planar, indicating that upon coordination the aromaticity of the phenyl rings is retained. The distortion from octahedral geometry is mainly caused by the acute bite angles involving the tetrahydrofuran oxygen O(1). The O(1)–Fe(1)–O(15) and O(23)–Fe(1)–O(45) angles are 166.00(8)° and 167.61(8)°, respectively, while the corresponding O(41)–Fe(1)–N(7) angle at 170.17(9)° also deviates from linearity. All the C–O bond lengths found in complex **1** are unremarkable, average 1.337(5) Å.

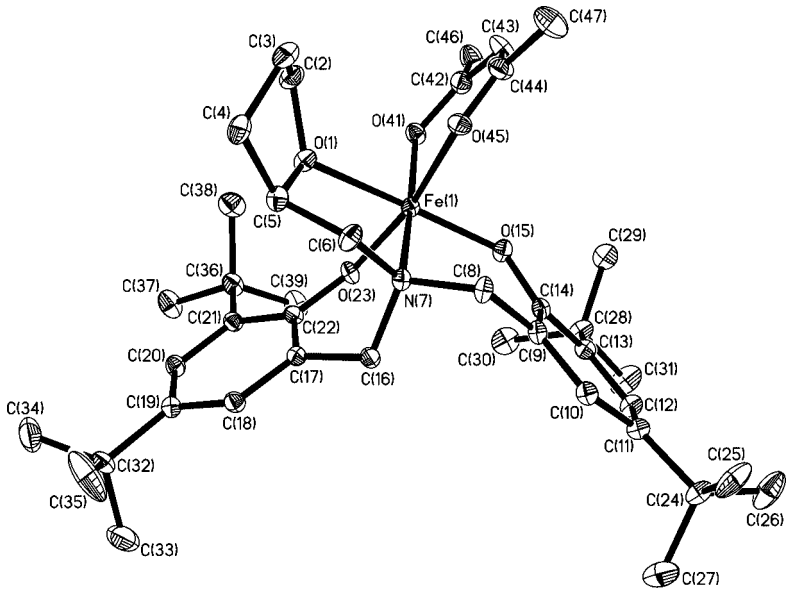

Figure 2. ORTEP diagram and atom labeling scheme for complex **1** (thermal ellipsoid probability 40%).

Table 2. Selected bond lengths [Å] and bond angles [°] for complex **1**·Et_2O.

Fe(1)–O(15)	1.883(2)	O(15)–Fe(1)–O(23)	99.20(9)
Fe(1)–O(23)	1.8891(19)	O(15)–Fe(1)–O(41)	95.53(8)
Fe(1)–O(41)	1.989(2)	O(23)–Fe(1)–O(41)	96.29(8)
Fe(1)–O(45)	2.0728(19)	O(15)–Fe(1)–O(45)	92.45(9)
Fe(1)–N(7)	2.193(2)	O(23)–Fe(1)–O(45)	167.61(8)
Fe(1)–O(1)	2.223(2)	O(41)–Fe(1)–O(45)	86.70(8)
O(15)–Fe(1)–N(7)	89.75(8)	O(15)–Fe(1)–O(1)	166.00(8)
O(23)–Fe(1)–N(7)	90.79(8)	O(23)–Fe(1)–O(1)	87.66(8)
O(41)–Fe(1)–N(7)	170.37(9)	O(41)–Fe(1)–O(1)	95.83(8)
O(45)–Fe(1)–N(7)	85.03(8)	O(45)–Fe(1)–O(1)	80.07(8)
N(7)–Fe(1)–O(1)	77.89(8)		
Fe(2)–O(73)	1.882(2)	O(73)–Fe(2)–O(65)	101.18(9)
Fe(2)–O(65)	1.896(2)	O(73)–Fe(2)–O(91)	95.17(9)
Fe(2)–O(95)	2.083(2)	O(65)–Fe(2)–O(91)	96.46(8)
Fe(2)–N(57)	2.187(2)	O(73)–Fe(2)–O(95)	90.07(9)
Fe(2)–O(51)	2.218(2)	O(65)–Fe(2)–O(95)	168.17(9)
Fe(2)–O(91)	1.988(2)	O(91)–Fe(2)–O(95)	86.03(9)
		O(73)–Fe(2)–N(57)	90.40(9)
		O(65)–Fe(2)–N(57)	89.55(9)
		O(91)–Fe(2)–N(57)	170.85(9)
		O(95)–Fe(2)–N(57)	86.71(9)
		O(73)–Fe(2)–O(51)	165.23(8)
		O(65)–Fe(2)–O(51)	87.53(8)
		O(91)–Fe(2)–O(51)	95.67(8)
		O(95)–Fe(2)–O(51)	80.71(8)
		N(57)–Fe(2)–O(51)	77.65(8)
C(22)–O(23)	1.341(3)		
C(14)–O(15)	1.326(3)		
C(64)–O(65)	1.336(3)		
C(72)–O(73)	1.343(3)		

It is noteworthy that the Fe(1)–O(1) bond length of 2.223(2) Å, involving the THF oxygen atom, is exceedingly long. This probably results in the comparatively short *trans*-positioned Fe(1)–O(15) bond length of 1.883(2) Å, thus indicating stronger Fe–O(phenolate) interactions in comparison to that for Fe–O(THF). The Fe(1)–N(7) distance at 2.193(2) Å falls into the range reported for the structurally characterized mononuclear Fe^{III} complexes.[8] The Fe–O and Fe–N bond lengths are in agreement with those of a high-spin d^5 Fe^{III} complex,[9] which corroborates also with the magnetic and Mössbauer measurements.

The structure of complex **2** consists of neutral, well-isolated dinuclear units $[L_2Fe^{III}_2(\mu\text{-}OH)(\mu\text{-}OCH_3)]\cdot C_2H_5\text{-}OC_2H_5$. Selected bond lengths and angles are listed in Table 3. An ORTEP view of the dimeric unit is shown in Figure 3. The two iron(III) atoms are asymmetrically bridged by one methoxy O(81) and one hydroxy O(80) ligands. The iron ion Fe(2) is in distorted octahedral environment, having $FeNO_5$ coordination sphere, whereas five-coordinate Fe(1) is in a square pyramidal $FeNO_4$ environment. The phenolate O(63), the amine N(47) and the bridging O(81) and O(80) form the equatorial plane for the Fe(2) center, whereas the phenolate O(55) and O(41) from the tetrahydrofuran unit are axially *trans*-disposed. As expected for *trans*-influence, the Fe(2)–O(41) distance is long with 2.207(5) Å, while the *trans*-bonded Fe(2) is hydrogen-bonded to the bridging hydroxide O(80). Thus, a distorted square-pyramidal Fe(1) prevails in complex **2**. The $FeNO_4$ coordination sphere is not very common for trivalent iron with O,N-based ligation,[10] octahedral coordination is by far the most commonly observed arrangement for Fe^{III}.[11] The bond lengths for the five-coordinate iron center Fe(1) is shorter than those for the six-coordinate Fe(2) center. The asymmetry in the bridging bond lengths is also noteworthy. The angles Fe(1)–O(81)–Fe(2) and Fe(1)–O(80)–Fe(2) at the bridging ligands are 103.3(1)° and 101.5(3)°, respectively and comparable with the reported values for similarly bridged iron(III) complexes.[12] The Fe(1)···Fe(2) separation of 3.116 Å fall in the range reported earlier. The Fe–N and Fe–O bond lengths are consistent with d^5 high-spin electron configuration for both Fe^{III} centers with amine nitrogen and phenolate oxygen-donor ligands. The d^5 high-spin configuration has also been confirmed both by Mössbauer and magnetic susceptibility measurements.

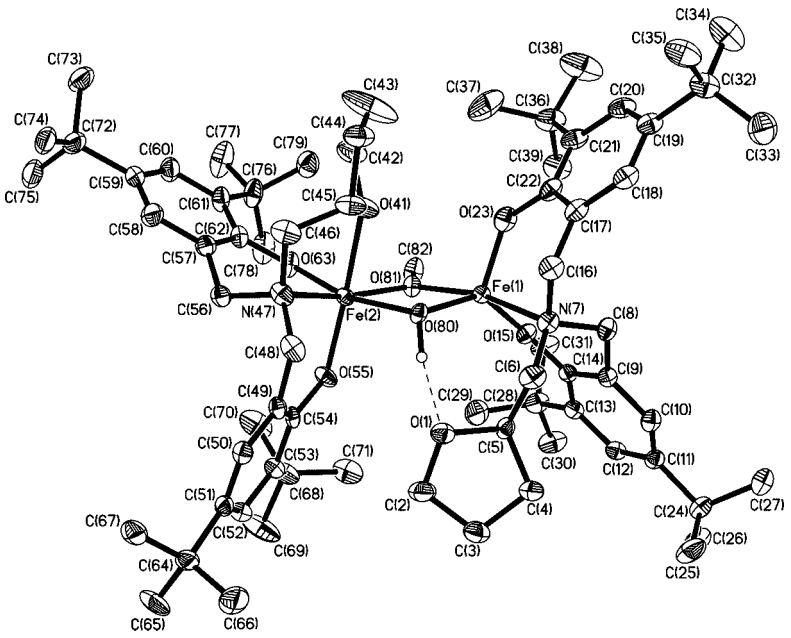

Figure 3. ORTEP diagram and atom labeling scheme for complex **2** (thermal ellipsoid probability 40%).

Table 3. Selected bond lengths [Å] and angles [°] for complex **2**·Et_2O.

Fe(1)–O(23)	1.796(2)	O(23)–Fe(1)–O(15)	108.21(9)
Fe(1)–O(15)	1.9172(19)	O(23)–Fe(1)–O(80)	113.67(19)
Fe(1)–O(80)	1.946(7)	O(23)–Fe(1)–O(81)	97.77(9)
Fe(1)–O(81)	1.983(2)	O(15)–Fe(1)–O(81)	96.65(9)
Fe(1)–N(7)	2.210(2)	O(80)–Fe(1)–O(81)	78.95(19)
Fe(2)–O(55)	1.887(3)	O(23)–Fe(1)–N(7)	92.58(8)
Fe(2)–O(63)	1.910(3)	O(15)–Fe(1)–N(7)	88.55(8)
Fe(2)–O(81)	1.991(2)	O(80)–Fe(1)–N(7)	87.27(18)
Fe(2)–O(80)	2.075(6)	O(81)–Fe(1)–N(7)	164.31(9)
Fe(2)–N(47)	2.196(2)	O(63)–Fe(2)–O(80)	165.8(3)
Fe(2)–O(41)	2.207(5)	O(55)–Fe(2)–O(80)	92.5(2)
O(55)–Fe(2)–O(63)	101.0(3)	O(81)–Fe(2)–O(80)	75.8(2)
O(55)–Fe(2)–O(81)	105.64(15)	O(55)–Fe(2)–N(47)	85.54(13)
O(63)–Fe(2)–O(80)	165.8(3)	O(81)–Fe(2)–N(47)	163.88(9)
O(81)–Fe(2)–O(80)	75.8(2)	O(55)–Fe(2)–O(41)	160.3(2)
O(63)–Fe(2)–N(47)	93.04(15)	O(81)–Fe(2)–O(41)	88.93(17)
O(80)–Fe(2)–N(47)	92.4(2)	N(47)–Fe(2)–O(41)	77.73(14)
O(63)–Fe(2)–O(41)	90.3(3)		
O(80)–Fe(2)–O(41)	78.1(3)		
Fe(1)–O(81)–Fe(2)	103.27(10)		

A perspective drawing of complex **3** [$L_2Fe^{III}_2(\mu\text{-}C_2O_4)$] and the atom-labeling Scheme are shown in Figure 4. Crystals of **3** contain two molecules of CH_2Cl_2 as solvent molecules of crystallization. Selected bond lengths and angles are given in Table 4. The asymmetric unit contains half of the dimer and consequently the geometries of the two iron centers are identical, with ligation provided by the two oxygen atoms of the bridging oxalate, two phenolate oxygens, one amine nitrogen and one ethereal oxygen belonging to the terminal ligand L resulting in a distorted octahedral arrangement. The two iron centers and the oxalate bridge are coplanar with a maximum deviation of 0.093 Å. As is expected and observed for the structures **1** and **2**, the Fe–O (ether) bond length at 2.178(2) is long and the *trans*-disposed Fe–O (phenolate) length at 1.867(2) Å is significantly short. The Fe–O and Fe–N bond lengths are in conformation with the high-spin d^5 electron configuration for the ferric centers in **3**, which corroborates with the Mössbauer and magnetic measurements. The Fe···Fe separation of 5.465 Å is comparable with those reported for other oxalate-bridged differic(III) complexes.[13]

Complex **4**·$C_2H_5OC_2H_5$ adopts a dimeric structure and the molecular structure is shown in Figure 5 along with the atom numbering scheme. Selected bond lengths and angles are listed in Table 5. Each copper atom has a $CuNO_4$ pentacoordinate environment and is bridged by two phenoxide oxygens O(15) and O(63). The Cu_2O_2 core is essentially planar, and none of the atoms deviates from the least-square plane by more than 0.38 Å. However, the Cu–O(63) and Cu–O(15) distances are different and the copper centers are separated by 2.766 Å, which is significantly shorter than those reported for phenoxy-bridged dicopper(II) complexes.[14]

The geometrical parameters τ of 0.31 and 0.29 for Cu(1) and Cu(2), respectively, suggest that the complex has a geometry closer to square-pyramidal (τ = 0) than to trigonal bipyramidal (τ = 1).[15] Thus, complex **4** adopts an folded structure with the two square-pyramidal copper centers bridged by the two phenoxide oxygen atoms, O(15) and O(63), with the Cu(1)–O–Cu(2) angles of 87.88(5)° and 88.65(5)°, respectively. The dispositions of the ligands are such that the equatorial tripodal nitrogen atoms N(7) and N(47), are in *syn* positions. Thus, the equatorial plane for each copper center consists of CuO_3N resulting from three phenolate oxygen atoms and the amine nitrogen atom. The oxygen atoms originating from the tetrahydrofuran arms of

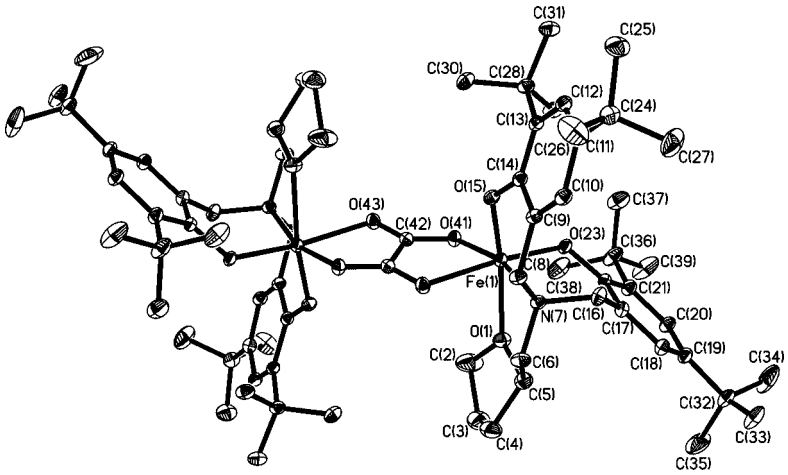

Figure 4. ORTEP diagram and atom labeling scheme for complex **3** (thermal ellipsoid probability 50%).

Table 4. Selected bond lengths [Å] and bond angles [°] for complex **3**·2CH_2Cl_2.

Fe(1)–O(15)	1.8665(19)	Fe(1)–O(23)	1.8728(18)
Fe(1)–O(41)	2.0394(19)	Fe(1)–N(7)	2.155(2)
Fe(1)–O(43)	2.1747(19)	Fe(1)–O(1)	2.178(2)
O(43)–Fe(1)	2.1746(19)	N(7)–Fe(1)–O(43)	89.03(8)
O(15)–Fe(1)–O(1)	164.80(8)	O(23)–Fe(1)–O(1)	91.14(8)
O(41)–Fe(1)–O(1)	91.19(8)	N(7)–Fe(1)–O(1)	77.48(8)
O(43)–Fe(1)–O(1)	80.94(8)	O(15)–Fe(1)–O(23)	100.69(9)
O(15)–Fe(1)–O(41)	96.51(8)	O(23)–Fe(1)–O(41)	98.11(8)
O(15)–Fe(1)–N(7)	92.36(8)	O(23)–Fe(1)–N(7)	92.55(8)
O(41)–Fe(1)–N(7)	164.61(8)	O(15)–Fe(1)–O(43)	87.69(8)
O(23)–Fe(1)–O(43)	171.39(9)	O(41)–Fe(1)–O(43)	78.82(7)

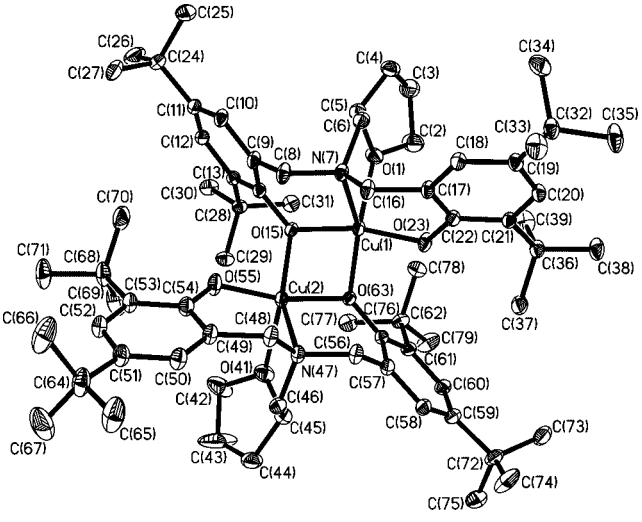

Figure 5. ORTEP diagram and atom labeling scheme for complex **4** (thermal ellipsoid probability 50%).

the aminebis(phenolate) ligand occupy the axial positions with *anti* conformation. As is observed for other structures, Cu–O (ether) bond is appreciably long with 2.334(5) Å and 2.400(4) Å.

Table 5. Selected bond lengths [Å] and angles [°] for complex **4**·$C_2H_5OC_2H_5$.

Cu(1)–O(23)	1.8780(14)	O(15)–Cu(1)–Cu(2)	47.12(4)
Cu(1)–O(15)	1.9571(13)	O(63)–Cu(1)–Cu(2)	44.58(4)
Cu(1)–O(63)	2.0156(13)	O(55)–Cu(2)–O(63)	167.41(6)
Cu(1)–N(7)	2.0482(16)	O(55)–Cu(2)–O(15)	92.65(6)
Cu(1)–O(1)	2.334(5)	O(63)–Cu(2)–O(15)	74.81(5)
Cu(1)–O(1X)	2.343(9)	O(55)–Cu(2)–N(47)	96.94(7)
Cu(2)–O(55)	1.8723(15)	O(63)–Cu(2)–N(47)	93.63(6)
Cu(2)–O(63)	1.9418(13)	O(15)–Cu(2)–N(47)	149.94(6)
Cu(2)–O(15)	2.0280(14)	O(55)–Cu(2)–O(41X)	89.3(3)
Cu(2)–N(47)	2.0543(17)	O(63)–Cu(2)–O(41X)	99.9(3)
Cu(2)–O(41X)	2.291(11)	O(15)–Cu(2)–O(41X)	132.3(2)
Cu(2)–O(41)	2.400(4)	N(47)–Cu(2)–O(41X)	76.4(3)
O(23)–Cu(1)–O(15)	167.37(6)	O(55)–Cu(2)–O(41)	98.10(9)
O(23)–Cu(1)–O(63)	92.66(6)	O(63)–Cu(2)–O(41)	90.52(8)
O(15)–Cu(1)–O(63)	74.76(5)	O(15)–Cu(2)–O(41)	127.24(9)
O(23)–Cu(1)–N(7)	95.90(6)	N(47)–Cu(2)–O(41)	79.52(9)
O(15)–Cu(1)–N(7)	84.46(6)	Cu(1)–O(15)–Cu(2)	87.88(5)
O(63)–Cu(1)–N(7)	148.77(6)	Cu(1)–O(63)–Cu(2)	88.65(5)
O(23)–Cu(1)–O(1)	99.77(11)	Cu(1)···Cu(2)	2.7658(3)
O(15)–Cu(1)–O(1)	89.37(10)		
O(63)–Cu(1)–O(1)	129.51(11)		
N(7)–Cu(1)–O(1)	78.42(11)		
O(23)–Cu(1)–O(1X)	90.8(2)		
O(15)–Cu(1)–O(1X)	98.2(2)		
O(63)–Cu(1)–O(1X)	130.59(18)		
N(7)–Cu(1)–O(1X)	79.36(19)		
O(23)–Cu(1)–Cu(2)	122.29(5)		

Mössbauer Isomer Shifts and Quadrupole Splittings

The zero-field Mössbauer spectrum of solid **1** at 80 K is broad and hence the spectrum was recorded in an applied field of 7 T at 4.2 K. This record shows a well-resolved six-line spectrum (Figure 6). A least-square fit of the spectrum yields isomer shift $\delta = 0.54$ mm·s^{-1} and quadrupole splitting $\Delta E_q = 1.55$ mm·s^{-1}. The Mössbauer data support the high-spin state of the ferric ion in a distorted octahedral field for complex **1** and are in agreement with the structural data.

Analysis of the zero-field Mössbauer spectra at 80 K for **2** and **3** yields the following parameters: isomer shift $\delta =$ 0.497 mm·s^{-1}, quadrupole splitting $\Delta E_q = 1.12$ mm s^{-1} for **2**

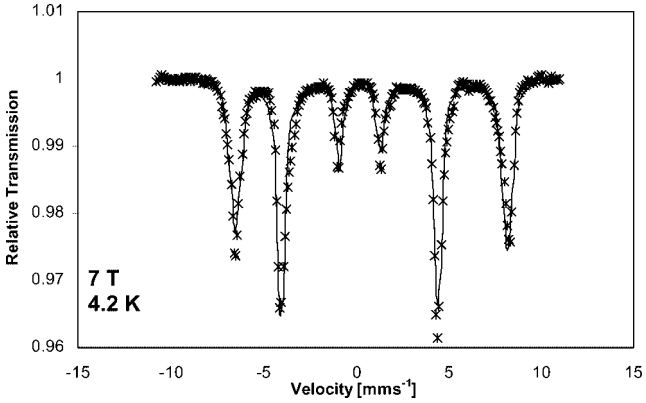

Figure 6. Mössbauer spectrum of **1** (applied field strength 7 T, T = 4.2 K.

and isomer shift δ = 0.531 mm s^{-1} and quadrupole splitting ΔE_q = 1.23 mm s^{-1} for **3**. These data indicate the presence of high-spin electronic configuration for the d^5 ferric(III) ions present in **2** and **3**.

Magnetic Susceptibility Measurements

Magnetic susceptibility data for polycrystalline samples of complexes **1**–**4** were collected in the temperature range 2–290 K in an applied magnetic field of 1 T. We start our discussion with the magnetic properties of the mononuclear complex **1**, [LFe^{III}(acac]. Complex **1** exhibits above 20 K essentially temperature-independent magnetic moment values μ_{eff} = 5.90 + 0.01 μ_B, and thus contains clearly a high-spin d^5 ion, h.s.Fe^{III}.

The magnetic behaviour of **2**, [$Fe_2L_2(\mu\text{-}OCH_3)(\mu\text{-}OH)$] is characteristic of an antiferromagnetically coupled dinuclear complex (Figure 7). At 290 K the μ_{eff} value of 7.76 μ_B ($\chi_M \cdot T$ = 7.5295 cm^3 K mol^{-1}) decreases monotonically with decreasing temperature until it reaches a value of 0.70 μ_B ($\chi_M \cdot T$ = 0.06127 cm^3 K mol^{-1}) at 1.9 K; this is a clear indication of exchange coupling between two paramagnetic high-spin Fe^{III} centers (S_{Fe} = $^5/_2$) with a resulting S_t = 0 ground state. We used the Heisenberg–Dirac–van Vleck spin-Hamiltonian in the form $\hat{H} = -2J\hat{S}_1 \cdot \hat{S}_2$ for an isotropic exchange coupling between two spins S_1 and S_2. The solid line in Figure 7 represents the best fit with the following parameters: J = –5.84 cm^{-1}, $g_1 = g_2$ = 2.00 (fixed) and TIP = 140 × 10^{-6} cm^3 mol^{-1} emu. The evaluated antiparallel exchange falls in the range observed for comparable diferric complexes containing alkoxo-, phenoxo- and hydroxo-bridges.[12] For comparison purposes, we report here some of our unpublished results on dibridged diferric(III) complexes **A**, **B**, **C**, and **D** comprising of six-coordinate Fe$^{III}_2(\mu\text{-}OH)_2$, 5-coordinated Fe$^{III}_2(\mu\text{-}OH)_2$, six-coordinate Fe$^{III}_2(\mu\text{-}OH)(\mu\text{-}$phenoxo) and six-coordinate Fe$^{III}_2(\mu\text{-}OCH_3)(\mu\text{-}$OAc), respectively.[16] Additionally, we have earlier reported a bis(μ-phenoxo)differic complex (**E**)[4a] containing a five-coordinate and a six-coordinate iron(III) center exhibiting an antiferromagnetic exchange coupling J = –7.4 cm^{-1}. Examination of **2** together with complexes **A**–**E** confirms the earlier notion about the exchange coupling ability of the bridging ligands following the trend $OH^- < OC_6H_5^- \approx OCH_3^-$. In addition, the strength of exchange coupling is weaker in five-coordinate Fe^{III} than that in six-coordinate species. The strongest coupling $|J|$ = 14.1 cm^{-1} observed for **D** with the widest bridging angle Fe(1)–O–Fe(2) of about 127°, resulting in an effective overlap between the metal and bridging-atom orbitals, is also in agreement with the existing magneto-structural correlation for the hydroxo-, alkoxo- and phenoxo-bridged diferric complexes.

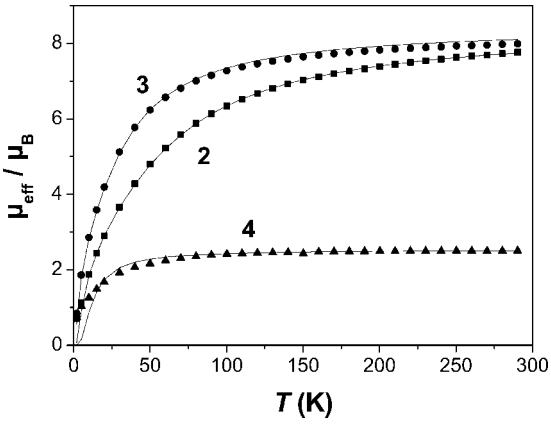

Figure 7. Magnetic measurements for complex **2**, **3** and **4**.

The μ_{eff} vs. T-plot for **3** is also shown in Figure 7 and indicates the nature of coupling operatiang between the two high-spin d^5 centers through the oxalate-bridge to be antiferromagnetic. The best parameters evaluated by simulation of the magnetic data are J = –3.1 cm^{-1}, g = 2.00. The exchange coupling constant in **3** compares well with those reported previously for oxalato-bridged dinuclear iron(III) complexes[13,17] and emphasizes the remarkable ability of the oxalate-bridge to transmit exchange interactions between paramagnetic centers separated by a distance more than 5 Å. It is noteworthy that structurally characterized oxalato-bridged differic(III) complexes are scarce in the literature.

The effective magnetic moment per molecule, μ_{eff}, for complex **4** (Figure 7) in the temperature range 290–90 K remains nearly constant, 2.50–2.39 μ_B, which is very close to the value of magnetic moment for two uncoupled spins of S = $^1/_2$. Below 90 K, μ_{eff} starts to decrease with decreasing temperature and reaches a value of μ_{eff} = 0.74 μ_B at 1.9 K. The observed temperature dependent magnetic moments for **4** confirms the dimeric nature with an antiferromagnetic exchange coupling of this compound. Simulation of these experimental data results in the following best fit parameters: J = –12.0 cm^{-1}, g = 2.05. The exchange coupling is much weaker than those reported for the bis(μ-phenoxide)dicopper(II) core, which in most of the cases is characterized by very strong antiferromagnetic interaction ($|J| \geq$ 100 cm^{-1}) with the Cu–O(Ph)–Cu angles ranging from 98.9° to 104.8°;[14] for examples of ferromagnetic coupling the Cu–O(Ph)–Cu angle lies in the range 90.8–96.1° and they are very rare.[14e,14i,14m] The remarkably weak antiferromagnetic interaction in **4** can be accounted for by con-

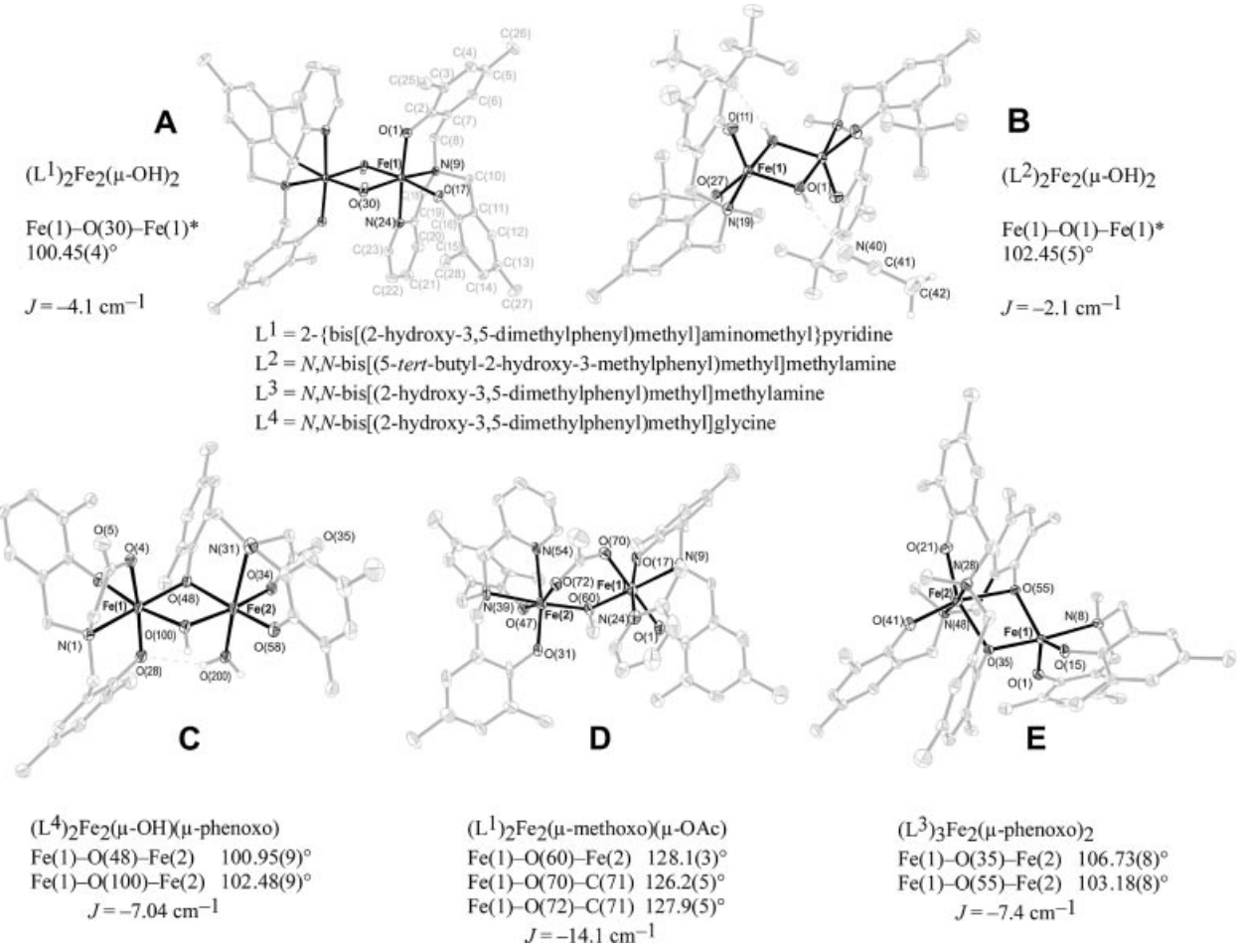

sidering the following major factors controlling the exchange interactions: (i) the equatorial planes of the copper centers, Cu(1)O(15)O(63)N(7)O(23) and Cu(2)O(63)N(47)O(55)O(15) are not planar with a dihedral angle of 81° between the planes, thus reducing the overlap of the magnetic orbitals of the copper centers via the *p*-orbitals of the bridging phenoxide oxygens; (ii) the angles at the bridging oxygen Cu–O(Ph)–Cu of about 88°, the smallest reported so far in the literature, result in considerable ferromagnetic contribution to the overall exchange interactions; (iii) the phenoxo oxygens, O(15) and O(63), adopt distorted pyramidal geometry (340.2° and 342.0°), thus increasing ferromagnetic contributions,[18] and (iv) small Cu···Cu distance of 2.766 Å also favors for decreasing the overall antiferromagnetic interaction by increasing ferromagnetism.[19] Hence, all these combined effects reduce the overall antiferromagnetic interactions drastically. It is remarkable that the Cu–O(Ph)–Cu angle at 88° for **4** with an antiferromagnetic coupling is even smaller than those for the ferromagnetically coupled diphenoxodicopper(II) complexes reported in the literature.[14e,14i,14m] These results suggest for a more intricate rationalization of exchange coupling in such phenoxo-bridged copper(II) complexes.

In this context we would like to point out that the Cu···Cu separation of 2.766 Å is the shortest known for bis(μ-phenoxide)dicopper(II) complexes. A similar bisphenoxo compound, $Cu_2L'_2$, (H_2L' = *N*,*N*-bis(2-hydroxylbenzyl)-*N*,*N*-dimethylethylenediamine) has been reported to exhibit a weak exchange coupling ($J = -10$ cm^{-1});[14h] the two copper centers in $Cu_2L'_2$ are in distorted trigonal-bipyramidal environments with the Cu–O(Ph)–Cu angle at 99.7° and the Cu(1)···Cu(1′) separation of 3.190 Å.

Electrochemistry and Spectroelectrochemistry

Cyclic- and square-wave voltammograms (CV and SQW) of complexes **1**–**4** have been recorded in CH_2Cl_2 solutions containing 0.2 M $[(n\text{Bu})_4\text{N}]PF_6$ as supporting electrolyte. A conventional three electrode arrangement was used, consisting of a glassy carbon working electrode, an $Ag/AgNO_3$ reference electrode and a platinum-wire counter electrode. Ferrocene was added as an internal standard after completion of a set of experiments, and potentials are referenced vs. the ferrocenium/ferrocene couple (Fc^+/Fc). Coulometric experiments were performed (at –25 °C) at appropriate fixed potentials to determine the number of electrons/molecule transferred in the redox process under investigation. During coulometry electronic spectra were recorded in order to obtain information about the mechanism of the redox process.

The CV and SQW voltammograms (Figure 8) observed with **1**–**4** revealed that each complex can be stepwise two times reversibly oxidized (E_1^{ox} and E_2^{ox} in Table 6). E_1^{ox} and E_2^{ox} are similar for **1**–**4**, which suggests that the oxidation mechanism might be the same for all complexes.

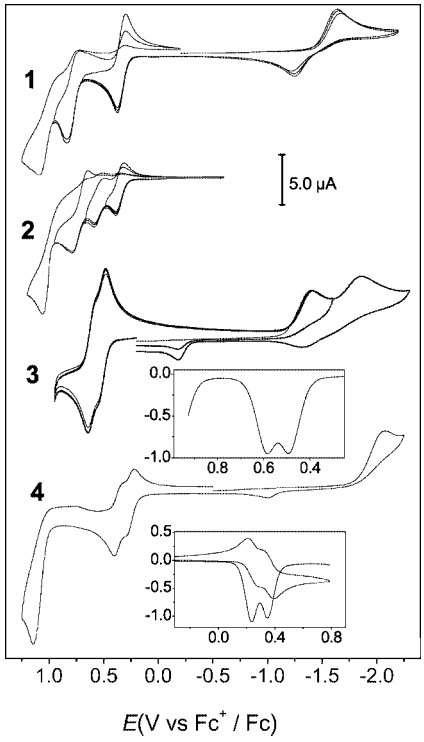

Figure 8. Cyclic and square-wave voltammogramms of complexes **1**–**4** in CH_2Cl_2 at room temperature.

Table 6. Electrode potentials (in Volt) for oxidation and reduction of complexes **1**–**4**, measured at ambient temperature in CH_2Cl_2 solutions and referenced vs. the Fc^+/Fc couple.

	E_4^{ox} /V	E_3^{ox} /V	E_2^{ox} /V	E_1^{ox} /V	E_{red} /V
1			+0.76[a]	+0.34[a]	–1.4[b]
2	+1.05[c]	+0.78[a]	+0.55[a]	+0.35[a]	–1.7[c]
3			+0.58[a]	+0.49[a]	–1.4[c]; –1.8[c]
4		+1.14[c]	+0.36[a]	+0.25[a]	–2.1[c]

[a] Reversible reaction, redox potential $E_{1/2}$ is given. [b] Electrochemical quasi-reversible reaction; estimated $E_{1/2}$ is given. [c] Irreversible reaction, peak potential is given.

In a coulometric experiment with the dimeric iron complex **3** it was found that 2 electrons per molecule had passed after completion of electrolysis at +0.8 V. The SQW voltammograms before and after coulometry were identical, indicating that the resulting monocation and dication were stable on the time scale of coulometry (20 min at –25 °C). The electronic spectral changes observed during $2e^-$ oxidation are shown in Figure 9. It is seen that the pattern of the changes is the same for both oxidation steps: a sharp band at 410 nm and a much broader one at 750 nm develop, which are typical for the formation of two phenoxyl radicals. Therefore the two oxidations are ligand centred. The small difference of the two redox potentials (90 mV) suggests that both ligands of the two respective iron-ions get mono-oxidized.

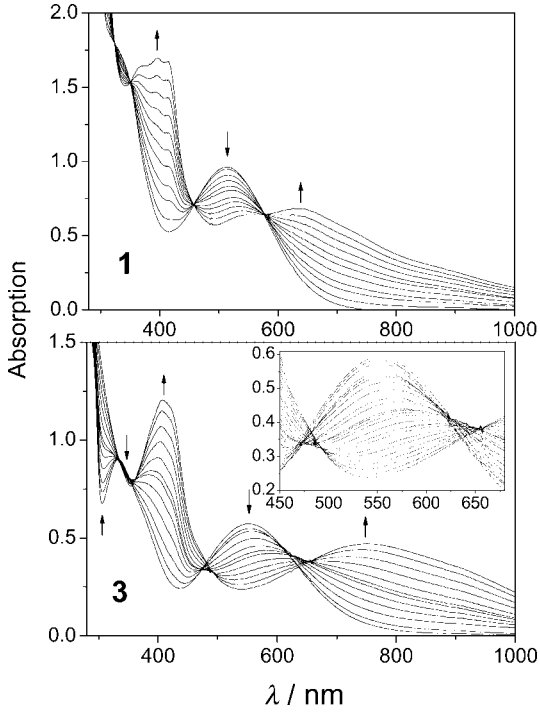

Figure 9. The electronic spectral changes during 1-e-oxidation for **1** and 2-e-oxidation for **3** (coulometry at T = –25 °C).

The CV of the dimeric copper complex **4** exhibits two reversible oxidations with a similar small difference in their redox potentials (110 mV) and also the absolute values of the redox potentials of this copper complex are similar to those of the iron complex **3**. Since furthermore the electronic spectrum of coulometrically generated monocation of **4** has a pronounced and sharp absorption band at 415 nm, we assume the same ligand centred oxidation mechanism for **4** as that for **3**.

The CV of the monomeric iron complex **1** exhibits at room temperature two oxidation waves of reversible appearance, followed by an irreversible oxidation (Figure 8). Already the dication, however, should be quite unstable, since the third oxidation is not observed at low temperatures (–25 °C) and, therefore, most possibly arises from a decomposition product of the dication. The monocation was stable under coulometric conditions and the UV/Vis absorption changes again indicate phenoxyl radical formation: an increase around 400 nm was observed and a new broad range centering around 630 nm (Figure 9).

All oxidized forms of **2** turned out to be unstable under coulometric conditions and, therefore, reliable spectroscopic data of them could not be obtained. However, the similarity of the redox potentials to those of the other complexes speaks again for ligand based oxidations.

At more positive potentials, the cyclic voltammograms of the dimeric complexes **2** and **4** show further oxidation waves, see Table 6. They are most possibly arising from oxidation of further phenolate moieties of the complexes, but there is no direct evidence for this interpretation.

In the negative potential range there are reductions discernible in the voltammograms which must be metal-centred. Only the Fe^{III}/Fe^{II} reduction of **1** is chemically reversible and occurs with a low rate of heterogeneous charge transfer, from the electrochemical view the reduction is quasi-reversible. This can be deduced from the high separation of the peaks of reduction and re-oxidation (ΔE_p). The separation is strongly dependent on the scan rate in a way that is typical of quasi-reversible reactions (ΔE_p = 0.53 V and 0.31 V at scan rates of 0.8 V/s and 0.05 V/s, respectively). The reductions of all other complexes are (chemically) irreversible, even on the time scale of cyclic voltammetry.

Concluding Remarks

The paper has described diversified ligating properties of a tetradentate ligand with [O,N,O,O] donor atoms. Both mononuclear and dinuclear complexes have been isolated and thoroughly studied. It has been shown that electrochemical oxidations are ligand-centered, i.e. formation of phenoxyl radicals from the coordinated phenolates.

Emphasis has been given in this work to structural and electronic effects arising from the incorporation of a pendent tetrahydrofuran moiety to the aminebis(phenolate) ligand, described earlier by us.[4] As expected the metal–O-(tetrahydrofuran) interactions are weak as judged by the comparatively long M–O(THF) distances. The use of a weak donor atom, THF-O, has made the isolation of an asymmetric diferric(III) complex containing a 5- and a six-coordinate ferric centers viable. A comparison with the hydroxo-, alkoxo- and phenoxo-bridged dinuclear Fe^{III} complexes from our laboratory has allowed us to judge the spin-exchange ability of the mentioned groups as exchange mediators. Moreover, for the diferric series it has been conclusively shown that the Fe–O–Fe angle is a major factor in determining the strength of the exchange interaction.

A bis(μ-phenoxo)dicopper(II) compound **4** with a remarkably weak antiferromagnetic exchange interaction (J = –12 cm^{-1}) along with the structural factors contributing to the weak interaction has been described. The copper(II) compound **4** is unique with the most short metal–metal separation of 2.766 Å and the smallest bridging angle Cu–O(Ph)–Cu of about 88° in the literature reported for bis(μ-phenoxo)dicopper(II) systems.

Experimental Section

Materials and Physical Measurements: Reagent or analytical grade materials were obtained from commercial suppliers and used without further purification, except those for electrochemical measurements. Elemental analyses (C,H,N) were performed by the Microanalytical Laboratory Dornis & Kolbe, Mülheim, Germany. Fourier transform infrared spectroscopy on KBr pellets was performed on a Perkin–Elmer 2000 FT IR instrument. Electronic absorption spectra in solution were measured on a Perkin–Elmer Lambda 19 spectrophotometer. Magnetic susceptibilities of *powdered samples* were recorded on a SQUID magnetometer in the temperature range 2–295 K with an applied field of 1 T. Experimental susceptibility data were corrected for the underlying diamagnetism using Pascal's constants and for the TIP contributions.

The Mössbauer spectrometer worked in the conventional constant-acceleration mode with a $^{57}Co/Rh$ source. Isomer shifts are given relative to α-Fe at room temperature (room temp.). Cyclic voltammetric and coulometric measurements were performed on EG&G equipment (potentiostat/galvanostat model 273A). Mass spectra were obtained with either a Finnigan MAT 8200 (electron ionization, EI MS) or a MAT 95 (electrospray ESI MS) instrument; a Bruker DRX 400 instrument was used for NMR spectra. Instrumental conditions for liquid chromatography are as follows: Shimadzu SPD-10 AV, Phenomenex Luna-5 C18, 150 × 4.6 mm column, UV 280 nm, eluent: CH_3OH/H_2O (9:1), room temp., sample size 5 μL, recording speed 0.5 cm min^{-1}.

Synthesis of H_2L: The ligand 2-{bis[(3,5-di-*tert*-butyl-2-hydroxybenzyl)amino]methyl}tetrahydrofuran was prepared as described in the literature.[6b] The purity (98.9%) of the ligand was checked by liquid chromatography; retention time 7.2 min for the eluent methanol with a flow rate of 0.8 mL min^{-1}; m.p. 148–149 °C. EI-MS: *m/z* (%) = 537 (32) [M^+], 466 (99.7) [$M^+ - C_4H_8O$], 219 (100) [$M^+ - C_{15}H_{23}O$]. ^1H NMR ($CDCl_3$): δ = 8.79 (br. s, 2 H), 7.24 (d, J = 2 Hz, 2 H), 6.86 (d, J = 2 Hz, 2 H), 4.26 (m, 1 H), 4.01 (m, 1 H), 3.88 (m, 1 H), 3.75 (m, 4 H), 2.60 (m, 1 H), 2.51 (m, 1 H), 1.91 (m, 3 H), 1.54 (m, 1 H), 1.40 (s, 18 H), 1.26 (s, 18 H) ppm. IR (KBr): $\tilde{\nu}$ = 3372 (s), 2963 (vs), 2867 (s), 1481 (s), 1443 (m), 1360 (s), 1302 (m), 1241 (s), 1217 (s), 1042 (m), 880 (s) cm^{-1}.

[LFe(acetylacetonate)], [LFe(acac)] (1): Solid $Fe(acac)_3$ (1 mmol, 0.35 g) was added to a solution of H_2L (1 mmol, 0.54 g) and Et_3N (2.8 mL) in distilled methanol (70 mL). The resulting red-orange solution was refluxed for 0.5 h, whereupon the color changed to dark red. On cooling a dark red solid precipitated. X-ray-quality crystals were grown by recrystallization from a 1:1 mixture of diethyl ether and methanol. Yield 0.47 g (68%). IR (KBr): $\tilde{\nu}$ = 2959, 2902, 1588, 1519, 1474, 1443, 1415, 1379, 1360, 1304, 1271, 1240, 1202, 1169, 1018, 976, 877, 838, 746 cm^{-1}. EI-MS: *m/z* (%) = 690 (47.7) [M^+], 591 (14) [$M - C_5H_7O_2$], 472 (100) [$M - C_{15}H_{23}O$], 372 (80) [$M - C_5H_7O_2 - C_{15}H_{23}O$]. UV/Vis ($CH_2Cl_2$): λ_{max} (ε, $M^{-1}cm^{-1}$) = 329 sh (8224), 517 (4620) nm. $Fe(C_{35}H_{53}NO_3)(C_5H_7O_2)$ (690.87): calcd. C 69.54, H 8.77, N 2.02, Fe 8.08; found C 69.4, H 8.2, N 2.0, Fe 8.1.

[L_2Fe_2(μ-OCH_3)(μ-OH)] (2): Dry $FeCl_2$ (1 mmol, 0.126 g) was added under argon to a thoroughly degassed methanolic solution (70 mL) of H_2L (1 mmol, 0.537 g), Et_3N (2.8 mL) and PPh_3 (2 mmol, 0.524 g). The resulting mixture was refluxed for 0.5 h resulting in a pale green solution, which upon exposure to air turned to dark red. The dark red solid was filtered and washed with methanol and air-dried. Yield 0.59 g (55%). X-ray-quality crystals were grown from a 1:1 solvent mixture of ether/methanol. IR (KBr): $\tilde{\nu}$ = 2954, 2902, 2868, 1602, 1471, 1439, 1413, 1361, 1274, 1239, 1203, 1169, 1132, 1067, 914, 874, 841, 809, 749 cm^{-1}. ESI-MS (positive mode, diethyl ether solution): *m/z* = 1201.7 (55) [$M^+ - OCH_3$], 591.3 (100) [$FeC_{35}H_{53}NO_3$]. UV/Vis (CH_2Cl_2): λ_{max} (ε, $M^{-1}cm^{-1}$) = 329 (12540), 465 (7560) nm. $C_{71}H_{110}Fe_2N_2O_8$ (1231.56): calcd. C 70.62, H 8.51, N 2.42, Fe 8.33; found C 69.2, H 9.0, N 2.3, Fe 9.0.

[L_2Fe_2(μ-C_2O_4)] (3): Solid $FeCl_2$ (1 mmol, 0.126 g) was added under argon to a degassed solution in methanol (70 mL) of H_2L (0.537, 1 mmol), Et_3N (5.4 mL) and oxalic acid (0.5 mmol, 0.06 g). The resulting mixture was stirred for 1 h and then exposed to air to yield a violet solution. The solution was filtered to get rid of any solid particles. The mother liquor was evaporated on a rotary evaporator to obtain a violet microcrystalline solid with an yield

of 0.51 g (40%). Violet single crystals were grown in a mixture of methanol/dichloromethane (1:1). IR (KBr): $\tilde{\nu}$ = 2952, 2903, 2869, 1655, 1470, 1443, 1438, 1414, 1304, 1268, 1241, 1170, 837, 7.33 cm^{-1}. ESI-MS (positive mode, CH_2Cl_2 solution): *m/z* = 1271 (68) [M^+]. UV/Vis (CH_2Cl_2): λ_{max} (ε, $M^{-1}cm^{-1}$) = 335 (10340), 554 (6620) nm. $C_{72}H_{106}Fe_2N_2O_{10}$ (1271.3): calcd. C 68.02, H 8.40, N 2.20, Fe 8.78; found C 67.8, H 8.3, N 2.2, Fe 8.7.

L_2Cu_2 (4): A methanolic solution (75 mL) of H_2L (1 mmol, 0.537 g) containing sodium methoxide (10 mmol, 0.54 g) was treated with solid $Cu(OAc)_2{\cdot}2H_2O$ (1 mmol, 0.199 g) and the resulting mixture was refluxed for 1 h whereupon a dark red solid appeared. The precipitate was collected by filtration, washed with methanol and air-dried; yield 0.74 g (62%). Red-brown single crystals were obtained from a mixture of diethyl ether/methanol (1:1). IR (KBr): $\tilde{\nu}$ = 2952, 2901, 2868, 1606, 1471, 1436, 1415, 1360, 1304, 1298, 1248, 1237, 1204, 1168, 1131, 1071, 1012, 875, 830, 740 cm^{-1}. EI-MS: *m/z* (%) = 1198 (1) [M^+], 598 (40) [$CuC_{35}H_{53}NO_3$]. UV/Vis (CH_2Cl_2): λ_{max} (ε, $M^{-1}cm^{-1}$) = 234 sh (8685), 423 (5260), ca. 730 (800) nm. $C_{70}H_{106}Cu_2N_2O_6$ (1198.9): calcd. C 70.13, H 8.91, N 2.34, Cu 10.6; found C 70.1, H 8.9, N 2.2, Cu 10.4.

X-ray Crystallographic Data Collection and Refinement of the Structures: Data collection for H_2L, **1**–**4**, was carried out on a Bruker-Nonius Kappa CCD diffractometer at 100(2) K by using graphite-monochromated Mo-K_α radiation (λ = 0.71073 Å). Final cell constants were obtained from a least-squares fit of all integrated reflections. Intensity data were corrected for Lorentz and polarization effects. The data sets for **1** and **2** were corrected for absorption (SADABS, Bruker-Nonius 2004).[20] The structures were solved by direct method and refined by full-matrix least-squares techniques based on F^2 (ShelXTL software package);[21] the neutral atom scattering factors of the program were used. Crystal data and refinement details are listed in Table 7.

Table 7. Crystallographic data for **1**·$C_2H_5OC_2H_5$, **2**·$C_2H_5OC_2H_5$ and **3**·$2CH_2Cl_2$.

	1	**2**	**3**
Empirical formula	$C_{42}H_{65}FeNO_{5.5}$	$C_{75}H_{120}Fe_2N_2O_9$	$C_{74}H_{110}Cl_4Fe_2N_2O_{10}$
Formula weight	727.80	1305.43	1441.14
Temperature /K	100(2)	100(2)	100(2)
Wavelength /Å	0.71073	0.71073	0.71073
Crystal system, space group	monoclinic, *Pc*, No. 7	monoclinic, $P2_1/c$, No. 14	monoclinic, $P2_1/n$, No. 14
Unit cell dimensions	a = 15.5080(8) Å, α = 90°	a = 15.5175(5) Å, α = 90°	a = 15.2801(5) Å, α = 90°
	b = 9.2357(5) Å, β = 104.059(5)°	b = 17.7071(6) Å, β = 100.105(5)°	b = 17.0204(6) Å, β = 103.123(5)°
	c = 29.535(2) Å, γ = 90°	c = 27.6524(10) Å, γ = 90°	c = 15.3018(5) Å, γ = 90°
Volume /Å^3	4103.5(4)	7480.2(4)	3875.7(2)
Z, D_c /Mg m^{-3}	4, 1.178	4, 1.159	2, 1.235
μ /mm–1	0.411	0.441	0.566
F(000)	1576	2832	1536
Crystal size /mm	0.14 × 0.04 × 0.03	0.18 × 0.06 × 0.04	0.06 × 0.06 × 0.02
Reflections collected/unique	57159–23295 [R(int) = 0.0497]	96609/17127 [R(int) = 0.0491]	98709/11707 [R(int) = 0.0680]
Absorption correction	Gaussian	Gaussian	none
Refinement method	full-matrix least-squares on F^2	full-matrix least-squares on F^2	full-matrix least-squares fit on F^2
Data/restraints/parameters	23295/21/937	17127/670/942	11707/30/434
Goodness-of-fit on F^2	1.072	1.047	1.236
Final R indices [$I > 2\sigma(I)$]	R_1 = 0.0560, wR_2 = 0.1120	R_1 = 0.616, wR_2 = 0.1435	R_1 = 0.0639, wR_2 = 0.1609
R indices (all data)	R_1 = 0.0785, wR_2 = 0.1215	R_1 = 0.0799, wR_2 = 0.1543	R_1 = 0.0728, wR_2 = 0.1645
Absolute structure parameter	not reliable		
Largest diff. peak and hole /e·A^{-3}	0.707 and –0.519	0.775 and –0.726	0.660 and –0.559
	H_2L	**4**·$C_2H_5OC_2H_5$	
Empirical formula	$C_{35}H_{55}NO_3$	$C_{74}H_{116}Cu_2N_2O_7$	
Formula weight	537.80	1272.77	
Temperature /K	100(2)	100(2)	
Wavelength /Å	0.71073	0.71073	
Crystal system, space group	orthorhombic, $P2_12_12_1$, No. 19	monoclinic, $P2_1/n$, No. 14	
Unit cell dimensions	a = 9.0712(6) Å, α = 90°	a = 18.8386(6) Å, α = 90°	
	b = 11.8239(8) Å, β = 90°	b = 15.2455(4) Å, β = 101.768(4)°	
	c = 31.201(2) Å, γ = 90°	c = 25.7956(8) Å, γ = 90°	
Volume /Å^3, Z	3346.5(4), 4	7252.9(4), 4	
D_c /Mg m^{-3}	1.067	1.166	
μ /mm^{-1}	0.066	0.637	
F(000)	1184	2752	
Crystal size /mm	0.22 × 0.20 × 0.12	0.24 × 0.20 × 0.06	
Reflections collected	31339	138783	
Independent reflections (R_{int})	6751 (0.0439)	23088 (0.0563)	
Absorption correction	not corrected	none	
Refinement method	full-matrix least-squares on F^2	full-matrix least-squares on F^2	
Data/restraints/parameters	6751–14–373	23088–161–861	
Goodness-of-fit on F^2	1.103	1.117	
Final R indices [$I > 2\sigma(I)$]	R_1 = 0.0543, wR_2 = 0.1328	R_1 = 0.0568, wR_2 = 0.1263	
R indices (all data)	R_1 = 0.0625, wR_2 = 0.1383	R_1 = 0.0715, wR_2 = 0.1328	
Absolute structure parameter	not reliable		
Largest diff. peak and hole /e·A^{-3}	0.197 and –0.163	1.171 and –1.042	

CCDC-634567 to -634571 (for **1**, **2**, **3**, **4** and H_2L, respectively) contain the supplementary crystallographic data for this paper. These data can be obtained free of charge from The Cambridge Crystallographic Data Centre via www.ccdc.cam.ac.uk/data_request/cif.

Acknowledgments

E. S. is thankful to the Max-Planck Gesellschaft and Iranian Ministry of Science, Research & Technology for a stipend. Thanks are due to Mrs. H. Schucht, Mrs. R. Wagner and Mr. A. Göbels for skilful technical assistance.

[1] a) J. Stubbe, W. A. van der Donk, *Chem. Rev.* **1998**, *98*, 705; b) R. H. Holm, E. I. Solomon, *Chem. Rev.* **1996**, 96; c) J. W. Whittaker, *Chem. Rev.* **2003**, *103*, 2347; d) J. Stubbe, *Chem. Commun.* **2003**, 2511; e) R. Banerjee, *Chem. Rev.* **2003**, *103*, 2081; f) H. Sigel, A. Sigel (Eds.), *Metal Ions in Biological Systems*, vol. 30, Marcel Dekker, New York, **1994**.

[2] Selected examples: a) J. A. Halfen, B. A. Jazdzewski, S. Mahapatra, L. M. Berreau, E. C. Wilkinson, L. Que Jr, W. B. Tolman, *J. Am. Chem. Soc.* **1997**, *119*, 8217; b) Y. Wang, T. D. P. Stack, *J. Am. Chem. Soc.* **1996**, *118*, 1309; c) D. Zurita, I. Gautier-Luneau, S. Menage, J. L. Pierre, E. Saint-Aman, *J. Biol. Inorg. Chem.* **1997**, *2*, 46; d) E. Bill, J. Müller, T. Weyhermüller, K. Wieghardt, *Inorg. Chem.* **1999**, *38*, 5795; e) Y. Shimazaki, S. Huth, A. Odani, Y. Yamauchi, *Angew. Chem. Int. Ed.* **2000**, *112*, 1666; f) S. Itoh, S. Takayama, R. Arakawa, A. Furuta, M. Kumatsu, A. Ishida, S. Takamuku, S. Fukuzumi, *Inorg. Chem.* **1997**, *36*, 1407; g) C. N. Verani, E. Bothe, D. Burdinski, T. Weyhermüller, U. Flörke, P. Chaudhuri, *Eur. J. Inorg. Chem.* **2001**, 2161.

[3] For example: a) P. Chaudhuri, K. Wieghardt, *Prog. Inorg. Chem.* **2001**, *50*, 151; b) S. Mukherjee, T. Weyhermüller, E. Bothe, K. Wieghardt, P. Chaudhuri, *Dalton Trans.* **2004**, 3842; c) T. K. Paine, T. Weyhermüller, K. Wieghardt, P. Chaudhuri, *Dalton Trans.* **2004**, 2092; d) P. Chaudhuri, K. Wieghardt, T. Weyhermüller, T. K. Paine, S. Mukherjee, C. Mukherjee, *Biol. Chem.* **2005**, *386*, 1023; e) C. Mukherjee, T. Weyhermüller, E. Bothe, P. Chaudhuri, *C. R. Chim.* **2007**, in press.

[4] a) T. Weyhermüller, T. K. Paine, E. Bothe, E. Bill, P. Chaudhuri, *Inorg. Chim. Acta* **2002**, *337*, 344; b) T. K. Paine, E. Rentschler, T. Weyhermüller, P. Chaudhuri, *Eur. J. Inorg. Chem.* **2003**, 3167.

[5] N. V. Timosheva, A. Chandrasekharan, R. O. Day, R. R. Holmes, *Inorg. Chem.* **1998**, *37*, 4945.

[6] a) E. Y. Tshuva, I. Goldberg, M. Kol, *J. Am. Chem. Soc.* **2000**, *122*, 10706; b) S. Groysman, I. Goldberg, M. Kol, E. Genizi, Z. Goldschmidt, *Inorg. Chim. Acta* **2003**, *345*, 137; c) J. Okuda, S. Fokken, T. Kleinhenn, T. P. Spaniol, *Eur. J. Inorg. Chem.* **2000**, 1321; d) E. Y. Tshuva, I. Goldberg, M. Kol, Z. Goldschmidt, *Inorg. Chem.* **2001**, *40*, 4263 and references cited therein.

[7] D. Armentano, G. De Munno, J. Faus, F. Lloret, J. Julve, *Inorg. Chem.* **2001**, *40*, 655.

[8] G. Wilkinson, R. D. Gillard, J. A. McCleverty (Editors), *Comprehensive Coordination Chemistry*, Pergamon Press, Oxford, **1987**.

[9] For example: a) B. S. Synder, G. S. Patterson, A. J. Abrahamson, R. Holm, *J. Am. Chem. Soc.* **1989**, *111*, 5214; b) P. Chaudhuri, M. Winter, P. Fleischhauer, W. Haase, U. Flörke, H.-J. Haupt, *Inorg. Chim. Acta* **1993**, *212*, 241.

[10] E. Bill, C. Krebs, M. Winter, M. Gerdan, A. X. Trautwein, U. Flörke, H.-J. Haupt, P. Chaudhuri, *Chem. Eur. J.* **1997**, *3*, 193.

[11] F. A. Cotton, G. Wilkinson, *Advanced Inorganic Chemistry*, Fifth Ed., Wiley, N. Y., **1988**.

[12] R. Werner, S. Ostrovsky, K. Griesar, W. Haase, *Inorg. Chim. Acta* **2001**, *326*, 78 and references cited therein.

[13] a) S. Rashid, S. S. Turner, P. Day, M. E. Light, M. B. Hursthouse, *Inorg. Chem.* **2000**, *39*, 2426; b) T. Fujino, Y. Hoshino, S. Igarashi, Y. Masuda, Y. Yukawa, *Inorg. Chim. Acta* **2004**, *357*, 11; c) M. Feist, S. Troyanov, E. Kemnitz, *Inorg. Chem.* **1996**, *35*, 3067; d) S. Triki, F. Bérézoksky, J. S. Pala, E. Coronado, C. J. Gómez-Garcia, J. M. Clemente, A. Riou, P. Molinie, *Inorg. Chem.* **2000**, *39*, 3771.

[14] Selected examples: a) B. Chiari, O. Piovesana, T. Tarantelli, P. F. Zanazzi, *Inorg. Chem.* **1988**, *27*, 4149; b) G. S. Speier, S. Tisza, Z. Tyeklár, C. W. Lange, C. G. Pierpont, *Inorg. Chem.* **1994**, *33*, 2041; c) L. K. Thompson, S. K. Mandal, S. S. Tandon, J. N. Bridson, M. K. Park, *Inorg. Chem.* **1996**, *35*, 3117; d) M. M. Whittaker, W. R. Duncan, J. W. Whittaker, *Inorg. Chem.* **1996**, *35*, 382; e) H. L. Shyu, H. H. Wei, G. H. Lee, Y. Wang, *Inorg. Chem.* **1996**, *35*, 5396; f) E. V. Rybak-Akimova, D. H. Busch, P. K. Kahol, N. Pinto, N. W. Alcock, H. J. Clase, *Inorg. Chem.* **1997**, *36*, 510; g) X.-H. Bu, M. Du, Z.-L. Shang, R.-H. Zhang, D.-Z. Liao, M. Shinoya, T. Clifford, *Inorg. Chem.* **2000**, *39*, 4190; h) H. Saimiya, Y. Sunatsuki, M. Kojima, S. Kashino, T. Kambe, M. Hirotsu, H. Akashi, K. Najajima, T. Tokii, *J. Chem. Soc., Dalton Trans.* **2002**, 3737; i) T. Kruse, T. Weyhermüller, K. Wieghardt, *Inorg. Chim. Acta* **2002**, *331*, 81; j) E. Berti, A. Caneschi, C. Daiguebonne, P. Dapporto, M. Formica, V. Fusi, L. Giorgi, A. Guerri, M. Micheloni, P. Paoli, R. Pontelfini, P. Rossi, *Inorg. Chem.* **2003**, *42*, 348; k) M. Thirumavalavan, P. Akilan, M. Kandaswamy, K. Chinnakali, G. S. Kumar, H. K. Fun, *Inorg. Chem.* **2003**, *42*, 3308; l) R. Paschke, S. Liebsch, C. Tschierske, M. A. Oakley, E. Sinn, *Inorg. Chem.* **2003**, *42*, 8230; m) S. Mukhopadhyay, D. Mandal, P. B. Chatterjee, C. Desplanches, J.-P. Sutter, R. J. Butchar, M. Chaudhury, *Inorg. Chem.* **2004**, *43*, 8501.

[15] A. W. Addison, T. N. Rao, J. Reedijk, J. van Rijn, G. Vershoor, *J. Chem. Soc., Dalton Trans.* **1984**, 1349.

[16] P. Chaudhuri, T. Weyhermüller, unpublished results.

[17] M. Julve, O. Kahn, *Inorg. Chim. Acta* **1983**, *76*, L39.

[18] V. H. Crawford, H. W. Richardson, J. R. Wasson, D. J. Hodgson, W. C. Hatfield, *Inorg. Chem.* **1976**, *15*, 2107.

[19] O. Kahn, *Inorg. Chim. Acta* **1982**, *62*, 3.

[20] G. M. Sheldrick, *SADABS Program for area detector absorption correction*, Institute for Inorganic Chemistry, University of Göttingen, Germany, **1996**.

[21] *SHELXTL 6.14 Version*, Bruker AXS, Karlsruhe, Germany.

Received: January 24, 2007
Published Online: April 25, 2007

